Genes and Environment, Vol. 31, No. 1 pp. 15–23 (2009)

Regular article

Knockdown of Severe Acute Respiratory Syndrome Corona Virus (SARS-CoV) Genes by Small Interfering RNA (siRNA) Using siRNA-expression Vectors and Synthetic Double-stranded RNA (dsRNA) as a Model for siRNA Design

Shizuyo Sutou[1,6], Miho Kunishi[1], Toshiyuki Kudo[1], Kenji Kawano[2], Yasuomi Takagi[2], Malgorzata Sierant[3], Masayuki Sano[4] and Makoto Miyagishi[5]

[1]School of Pharmacy, Shujitsu University, Okayama, Japan
[2]iGENE Therapeutics Inc., Tokyo, Japan
[3]Centre of Molecular and Macromolecular Studies, Polish Academy of Sciences, Department of Bioorganic Chemistry, Sienkiewicza, Poland
[4]Biotherapeutic Research Laboratory, National Institute of Advanced Industrial Science and Technology (AIST), Ibaraki, Japan
[5]Department of Gene Diagnostics and Therapeutics, Research Institute, International Medical Center of Japan, Tokyo, Japan

(Received October 10, 2008; Revised November 25, 2008; Accepted November 26, 2008)

While offering the promise of therapeutic use in the future, RNA interference (RNAi) technology is useful to knock down genes posttranscriptionally. We attempted to knock down severe acute respiratory syndrome (SARS)-corona virus (Cov) genes using small interfering RNA (siRNA) employing siRNA-expression vectors and synthetic double-stranded RNA (dsRNA) as a model for effective siRNA design. First, we selected three target sites without mutations among 15 SARS-Cov strains using a prediction algorithm and constructed three siRNA-expression vectors. Using a pGL3 vector, we constructed three corresponding model target vectors to the firefly luciferase gene (*Fluc*), to which the model targets were connected. Using *Renilla* luciferase gene (*Rluc*) as the internal control, the three siRNA vectors knocked down the targets, providing effective target sequences. Almost identical results were obtained when *Rluc* was integrated into the pGL3-Fluc target vector. Next, effective structures of synthetic double-stranded RNA (dsRNA) were investigated using two targets. In all, six RNAs per target were synthesized: complementary sense and antisense 19-mer core RNAs; sense 21-mer RNAs having a 2-nucleotide (nt) match or unmatch overhang at the 3′-end; and antisense 21-mer RNAs having a 2-nt match or unmatch overhang at the 3′-end. The six RNAs provided nine species of dsRNAs (a blunt 19-mer duplex, a total of 4 19-mer/21-mer duplexes with a match or unmatch 2-nt overhang at the 3′- end of the sense or antisense strand, 4 21-mer/21-mer duplexes with match or unmatch 2-nt overhang at both ends) in combination. Targets were sense or antisense sequences. Generally, 19-mer/21-mer dsRNA with a match 2-nt overhang at the 3′-end of the antisense strand showed the highest activity, irrespective of the thermodynamic stabilities at terminal ends, suggesting that the 2-nt overhang is more critical than thermodynamic stabilities to select the antisense strand to the RNA-induced silencing complex (RISC).

Key words: SARS-CoV, siRNA, RNAi, thermodynamic stability, 3′-end overhang

Introduction

Atypical pneumonia occurred in a Canton district in China in November 2002. At the same time, a new A/H5N1 type influenza virus was detected in Hong Kong. In March 2003, new patients were found in Vietnam, Hong Kong, Canada, Singapore, and Germany, but the influenza virus remained undetected. The World Health Organization (WHO) called the new disease severe acute respiratory syndrome (SARS). Immediately, WHO called for joint research with 11 facilities and discovered a new corona virus on March 27: the SARS corona virus (SARS-CoV) (1). By April 15, the genomic sequence of about 30,000 of SARS-CoV had been identified. The number of patients had reached 8,422 in 29 countries on August 7, 2003; deaths were 916 (11%) (WHO: http://www.who.int/csr/sars/en/). The SARS-CoV afflicts the whole body. It mainly affects the lungs, immune organs, and small blood vessels (2). Its economic loss was estimated as $100 billion or more because of the discontinuance of conferences and meet-

[6]Correspondence to: Shizuyo Sutou, School of Pharmacy, Shujitsu University, 1-6-1 Nishigawara, Okayama 703-8516, Japan. Tel/Fax: +81-86-271-8357, E-mail: sutou@shujitsu.ac.jp

ings, travel prohibitions, and decreased investment (3).

It is desirable to counteract emerging infectious diseases using a new technology, RNA interference (RNAi), where synthetic double-stranded RNA (dsRNA) is used to cleave mRNA sequence-specifically (4). In mammalian cells, longer dsRNA induces the interferon (IFN) response and RNAi is assumed to be nonfunctional. Short interfering RNA (siRNA), however, circumvents the IFN response (5). Many living organisms such as mammals, birds, plants, insects, fish, planarians, hydras, paramecia, spiders, tetrahymenas, chlamidomonases, neurosporas, trypanosomas, slime molds, and fission yeasts are equipped with the RNAi pathway. Functions of RNAi are diverse depending on the organism; major roles of RNAi are transposon silencing, viral defense, and gene regulation (6, and references therein). The therapeutic use of RNAi is anticipated for many diseases, including respiratory viral diseases such as SARS (7).

In fact, siRNA consists of two complementary strands of approximately 21 nucleotides (nts) with 2-nt overhangs at both 3′- ends (8). One strand of the duplex is designated as the ''passenger strand,'' which is later discarded, and the other ''guide strand'' is assembled into the RNA-induced silencing complex (RISC). Argonaute 2 (Ago2), the catalytic component of the RISC, catalyzes the cleavage of target mRNA between the tenth and eleventh nts measured from the 5′-end of the guide strand (9). In *Drosophila*, a heterodimer with *Drosophila* Dicer (Dcr-2) and dsRNA-binding partner R2D2 determines asymmetric loading of siRNA strands into the RISC (10). In fact, R2D2 binds to the 5′-end with a greater internal stability and directs the Dcr-2 to the 5′-end of the opposite strand to be loaded into the RISC. In mammalian cells, co-factor(s) interacting with Dicer might play an important role in the strand selection as in the fruit fly, but relevant details have not been established.

The genome of SARS-CoV consists of plus-stranded single RNA; genes with 14 ORFs are made up of a nested set (11). The virus belongs to the family Nidovirales, which is known for frequent mutations: a prior study presents an example (12). Difficulties for vaccine development posed by the high mutation rates necessitate effective anti-SARS drug development. To explore the possibility of interrupting SARS-CoV replication by RNAi, specific siRNAs targeting the viral spike (13), NP (14), RdRP (15,16) and envelope protein genes (17) as well as the leader sequence (18) were synthesized and introduced into mammalian cells. In these studies (13–18), siRNAs were apparently designed according to guidelines (8,19,20) that recommend 5′-AA(N_{19})UU (where N is any nucleotide) in mRNA as a preferred target sequence; the hybridization of 5′-(N_{19})UU-3′ and 3′-UU-(complementary N_{19})-5′ provides 19-bp dsRNA with a UU overhang at both 3′-ends. Furthermore, the 2-UU overhangs at both 3′-ends in the sense and antisense of dsRNA can be replaced by dTdT without adverse effects. If this motif is absent, 5′-AA(N_{21}) or 5′-NA(N_{21}) is allowed. Our approach differs from those of prior studies (13–18) in the following respects. First, making the most of the genomic structure, we searched for target sites at random over a whole SARS-CoV genome using a prediction algorithm (21). After omitting possible off-target—silencing of unintended transcripts in addition to the target gene—sequences, the best three candidate target sites without mutations were chosen from among 15 strains. Secondly, because symmetric structures with 3′-UU or 3′-dTdT might provide sense and antisense strands with an equal chance to be loaded into RISC, thereby lessening the effectiveness of siRNA, we studied the dsRNA end structures. Thirdly, we examined the relevance of reports that the lower thermodynamic stability at the 5′- end of antisense strand is critically important to load the antisense strand into RISC (22,23). We showed recently that a unilateral 3′-overhang at the antisense strand is more important than thermodynamic stabilities at siRNA ends (24). In the present study, we confirm the importance of the asymmetric structure of dsRNA and the 3′-overhang at the antisense strand. In addition, we examine the effective sequence of the overhang, which is expected to be complementary to its target mRNA, at least in the present model case of the SARS-CoV gene.

Materials and Methods

Prediction of optimal target sequences: The entire genomic sequence of a SARS-CoV strain was obtained from a database (NCBI registration no.: NC_004718). Optimal target sites, #1 ~ #3 were predicted using a program (21). The other SARS-CoV strains—AY278491, AY310120, AY278489, AY362699, AY283798, AY278741, AY351680, AP006561, AY278554, AY348314, AY323977, AY323977, AY279354, and AY297028—include no mutations in the three target site sequences (Table 1).

Construction of reporter vectors with a model target sequence: Because a P3 level facility was not available to us, we were unable to use a live SARS-CoV virus; model target vectors were constructed. One of

Table 1. Selected target sites and their sequences

Target site (nucleotide number*)	Prediction score	Sequence
#1 (674–692)	0.865	5′-GCAUCGAUCUAAAGUCUUA-3′
#2 (13721–13739)	0.8855	5′-GCGUCUAACUAAAUACACA-3′
#3 (17899–17917)	0.8741	5′-AUAGAGAUCUUUAUGACAA-3′

*Nucleotide number of SARS-CoV (NC_004718).

Table 2. List of vectors

Vector name	Description	Associated figure
piGENE hU6	siRNA expression vector (negative control)	Figs. 1, 2, 3
pRL-TK	*Rluc* expression vector (internal control)	Figs. 1, 2, 3, 4, 5, 6
SARS#1	Target vector harboring the #1 sequence	Figs. 1, 4
SARS#2	Target vector harboring the #2 sequence	Figs. 1, 2, 3
SARS#3	Target vector harboring the #3 sequence	Figs. 1, 5, 6
R-SARS#1	Target vector harboring the reverse sequence of SARS#1	Fig. 4
R-SARS#3	Target vector harboring the reverse sequence of SARS#3	Figs. 5, 6
SARS#2-Rluc	*Rluc* was integrated into SARS#2 as the internal control.	Fig. 3
siRNA#1	siRNA expression vector targeting #1	Figs. 1, 2, 4
siRNA#2	siRNA expression vector targeting #2	Figs. 1, 2, 3
siRNA#3	siRNA expression vector targeting #3	Figs. 1, 2, 5, 6

them, which has the target sequence starting from 674 of NC 004718 (#1), is shown here as an example. First, the multiple cloning site upstream of the SV40 promoter was removed from the pGL3-control vector (Promega Corp., Madison, MI) by cutting with restriction enzymes *Kpn*I and *Bgl*II. The vector DNA was treated with T4 DNA polymerase to blunt the cut ends; then with T4 DNA ligase to make it circular. Second, a multiple cloning site (*Xba*I, *Aat*II, *Bgl*II, *Sal*I, *Pst*I, *Apa*I, *Sma*I/*Xma*I, *Spe*I, *Afl*II, and *Spl*I) was created at the *Xba*I site just behind the stop codon of the firefly luciferase gene (*Fluc*). Third, two 72-mer DNAs (indicated below) that harbored the target sequence (italicized capital letters) were synthesized; the two were annealed (complementary sequences are underlined). Then DNA was treated with Klenow fragment to make double-stranded DNA.

5′-AAGCTTgtcgacTAAGAACGGTAATAAGGGAG-CCGGTGGTCATAGCTATGGC*ATCGATCTAAAG-TCTTATGA*-3′

5′-AAATTTactagtATAATCTTCAATGGGATCAGT-GCCAAGCTCGTCACCTAAGTCATAAGACTTTA-GATCGAT-3′

Then the DNA was digested with restriction enzymes *Sal*I and *Spe*I (their target sites are shown in lower case letters). It was connected to the reporter vector DNA that had been cut with the same restriction enzymes. Consequently, the model reporter vector, harboring the target sequence consisting of approximately 100-bp, was constructed. Model target vectors with sequences of #2 and #3, starting from 13721 and 17899 respectively, were also constructed using the same method. Constructed vectors are listed in Table 2 as SARS#1, SARS#2, and SARS#3.

Construction of reporter vectors with a reverse target sequence: Reporter vectors harboring the opposite target sequence were constructed using the same method as described above to determine the activity of the sense strand. We constructed two models with approximately 100-bp sequences starting from 674 and 17899. Constructed vectors are listed in Table 2 as R-SARS#1 and R-SARS#3.

Construction of siRNA expression vectors: The siRNA expression vectors were constructed using the piGENE hU6 vector (iGENE Therapeutics Inc., Tokyo). The stem sequence was 22 base pairs (bp), which is one of the most effective lengths (25). For instance, two single-strand DNAs shown below were synthesized to produce a 22-mer siRNA targeting the sequence GCAUCGAUCUAAAGUCUUAUGA (#1 site of SARS-CoV, NC_004718).

5′-CACC GCATtGATCTAgAGTCTTgTGA
cttcctgtgca
TCATAAGACTTTAGATCGATGC TTTTT-3′
3′-CGTAaCTAGATcTCAGAAcACT gaaggacacgt
AGTATTCTGAAATCTAGCTACG AAAAA
TACG–5′

The two were annealed, producing terminal 4-nt 5′-extrusions that were compatible with *Bsp*MI-cut ends. Subsequently, DNA was ligated to piGENE hU6 cut with *Bsp*MI. In fact, GCATtGATCTAgAGTCTTgTGA corresponds to the target sequence, in which three mutations shown in lower case letters were introduced to avoid recombinations in the host *E. coli*, and also to avoid sequencing difficulties. A loop structure is presented in 11 lower case letters in the middle; TTTTT is the stop signal to RNA pol III. The siRNA expression vectors targeting sequences starting from 13721 (#2) and 17899 (#3) were constructed similarly. Constructed vectors are listed in Table 2 as siRNA#1, siRNA#2, and siRNA#3.

Internal control and construction of reporter vectors harboring the internal control: In one series of experiments, pRL-TK (Promega Corp.) harboring *Renilla* luciferase gene (*Rluc*) was used as the internal control. In another series of experiments, the internal control was integrated into the pGL3-based target vector. We constructed the pGL3-based plasmid harboring *Rluc* that was targeting the bovine prion gene (b*PRNP*) (25). The b*PRNP* fragment was replaced with the SARS fragment starting from No. 13719 using *Aat*II and *Spl*I sites. The promoter of *Rluc* is that of thymidine kinase

Table 3. Structures of dsRNAs

Combinations	End structure*	Sequence
[1]–[2]	b-b	5′-AUAGAGAUCUUUAUGACAA-3′ 3′-UAUCUCUAGAAAUACUGUU-5′
[1]–[5]	m-b	5′-AUAGAGAUCUUUAUGACAA-3′ 3′-acUAUCUCUAGAAAUACUGUU-5′
[1]–[6]	u-b	5′- AUAGAGAUCUUUAUGACAA-3′ 3′-guUAUCUCUAGAAAUACUGUU-5′
[2]–[3]	b-m	5′-AUAGAGAUCUUUAUGACAAac-3′ 3′-UAUCUCUAGAAAUACUGUU-5′
[2]–[4]	b-u	5′-AUAGAGAUCUUUAUGACAAgu-3′ 3′-UAUCUCUAGAAAUACUGUU-5′
[3]–[5]	m-m	5′-AUAGAGAUCUUUAUGACAAac-3′ 3′-acUAUCUCUAGAAAUACUGUU-5′
[3]–[6]	u-m	5′-AUAGAGAUCUUUAUGACAAac-3′ 3′-guUAUCUCUAGAAAUACUGUU-5′
[4]–[5]	m-u	5′-AUAGAGAUCUUUAUGACAAgu-3′ 3′-acUAUCUCUAGAAAUACUGUU-5′
[4]–[6]	u-u	5′-AUAGAGAUCUUUAUGACAAgu-3′ 3′-guUAUCUCUAGAAAUACUGUU-5′

*b, blunt; m, match overhang; u, unmatch overhang. The left letter indicates the left end and the right letter the right end.

of a herpes virus, whereas that of *Fluc* is SV 40. The vector is listed in Table 2 as SARS-Rluc.

Construction of dsRNA: As an example, the construction of synthetic dsRNA targeting the sequence starting from 17899 (SARS#3) is described. The sequence around the target (underlined) is: 5′-TAATGTCTGATAGAGATCTTTATGACAAACTG-CAATTTAC-3′. Based on the stem 19-mer, six sense and antisense RNAs with or without a 2-nt match or unmatch 3′-overhang were synthesized. They are listed below. The match overhang means that the 2-nt is matched to the target mRNA in the sense strand or that it is complementary to the mRNA in the antisense strand. The unmatch overhangs means that adenine (a) is replaced with guanine (g) and cytosine (c) is replaced with uracil (u) so that the overhangs are not complementary to the target mRNA.

[1] Basic sense 19-mer:
5′-AUAGAGAUCUUUAUGACAA-3′
[2] Basic antisense 19-mer:
3′-UAUCUCUAGAAAUACUGUU-5′
[3] Sense 21-mer with a 3′-2 nt match overhang:
5′-AUAGAGAUCUUUAUGACAAac-3′
[4] Sense 21-mer with a 3′-2 nt unmatch overhang:
5′-AUAGAGAUCUUUAUGACAAgu-3′
[5] Antisense 21-mer with a 3′-2 nt match overhang:
3′-acUAUCUCUAGAAAUACUGUU-5′
[6] Antisense 21-mer with a 3′-2 nt unmatch overhang:
3′-guUAUCUCUAGAAAUACUGUU-5′

In all, nine dsRNAs in combinations of the six were constructed by annealing [1] and [2], [1] and [5], [1] and [6], [2] and [3], [3] and [5], [3] and [6], [2] and [4], [4] and [5], and [4] and [6] (Table 3). Similarly, nine dsRNAs targeting the sequence starting from 674 (#1) were constructed.

Measurement of RNAi activity: Typically, RNAi activity was measured as follows: HeLa cells were plated in a 24 or 48 well plate with Dulbecco's minimal essential medium (DMEM) supplemented with 10% fetal calf serum. Target vector DNA, internal control DNA (pRL-TK; Promega Corp.), and siRNA expression vector DNA or various dose levels of synthetic dsRNA were mixed with lipofectamine 2000 (Invitrogen Corp., Carlsbad, CA, U.S.A.), and added to the culture. After 24 h, cells were lysed with 100 μL of lysis buffer (Promega Corp.). The luminescence of *Fluc* and *Rluc* was measured with Sirius Luminometer (Berthold Detection Systems GmbH, Pforzheim, Germany) using a Dual Luciferase Reporter Assay System (Promega Corp.) according to the manufacturer's instruction. Briefly, an aliquot (5 μL) of the lysed sample was added to 25 μL of Dual-Glo Luciferase Substarte solution in a 1.5 mL snap-cap microcentrifuge tube, and the intensity of luminescence of *Fluc* was measured. Then 25 μL of Dual-Glo Stop and Glo Substrate solution were added to the mixture, and the intensity of luminescence of *Rluc* was measured. The Dual-Glo Luciferase Substrate solution was a component of the Assay kit, and the Dual-Glo Stop and Glo Substrate solution was prepared just before use by mixing Dual-Glo Stop and Glo Buffer and Dual-Glo Stop and Glo Substrate (50:1) as indicated.

Calculation of terminal thermodynamic stability (ΔG): Terminal thermodynamic stability (ΔG) was calculated according to the thermodynamic parameters for terminal 4-bp (26).

Results

Effects of siRNA expression vectors on model targets: All three siRNA expression vectors efficiently knocked down each model target (Fig. 1). The effectiveness of the three was in the order of siRNA#2 > siRNA#3 > siRNA#1. The order reflects the predicted scores exactly, suggesting the usefulness of the prediction algorithm (Table 1).

Target sequence specificity: When siRNA expression vectors siRNA#1 and siRNA#3 challenged the model target SARS#2, neither siRNA#1 nor siRNA#3 showed knockdown activity, indicating sequence-specific targeting of siRNA against mRNA (Fig. 2).

Comparison of separate and integrated internal controls: The siRNA activities were measured in the presence of three DNAs–target, internal control, and siRNA expression vector–in experiments depicted in Figs. 1 and 2. To avoid experimental complexity, the internal control was integrated into the target vector. A simplified assay, in which the target and siRNA expression vector DNAs were added, was carried out. Almost

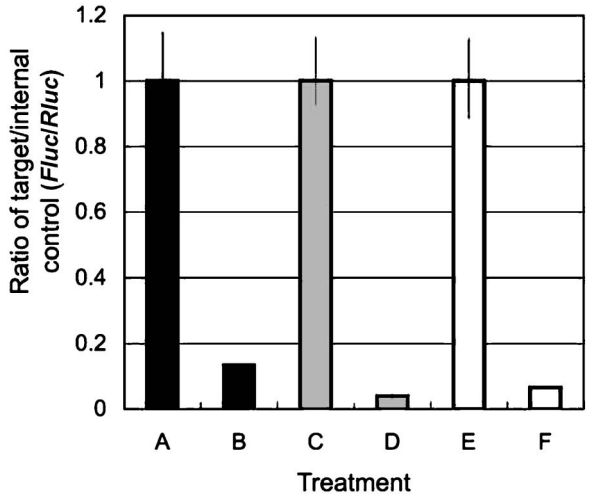

Fig. 1. Effects of siRNA expression vectors on their reporter model target vectors. HeLa cells (7.5×10^4/well in a 24-well plate) were treated with SARS#1, piGENE hU6, and pRL-TK (A), SARS#1, siRNA#1, and pRL-TK (B), SARS#2, piGENE hU6, and pRL-TK (C), SARS#2, siRNA#2, and pRL-TK (D), SARS#3, piGENE hU6, and pRL-TK (E), or SARS#3, siRNA#3, and pRL-TK (F) as described in materials and methods. A concentration of 100 ng DNA/well was used for all plasmid vectors. SARS#1, SARS#2, and SARS#3 denote target vectors harboring targeting sequences of #1, #2, and #3 of SARS-CoV, NC_004718, respectively. siRNA#1, siRNA#2, and siRNA#3 signify siRNA expression vectors targeting sequences of #1, #2 and #3, respectively (see Tables 1 and 2). Bars indicate means and ranges of *Fluc/Rluc* ratios.

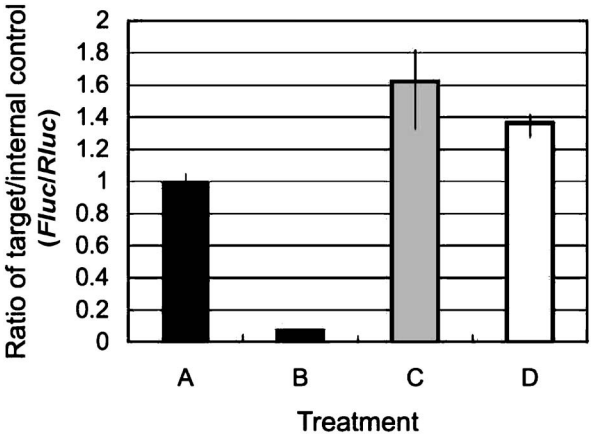

Fig. 2. Sequence-specific targeting of siRNA expression vectors. HeLa cells (1.5×10^4/well in a 48-well plate) were treated with SARS#2, piGENE hU6, and pRL-TK (A), SARS#2, siRNA#2, and pRL-TK (B), SARS#2, siRNA#1, and pRL-TK (C), or SARS#2, siRNA#3, and pRL-TK (D). A concentration of 100 ng DNA/well was used for vectors SARS#1, SARS#2, SARS#3, and piGENE hU6, and that of 50 ng DNA/well, for pRL-TK. As for vectors and target sequences, see Tables 1 and 2.

identical activities were obtained (Fig. 3). Therefore, the target vector containing the internal control is convenient. No differences in activities were seen between

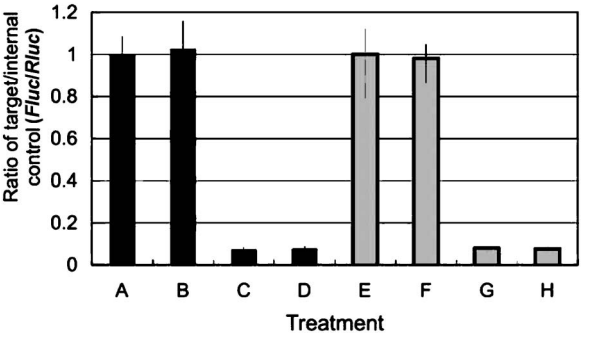

Fig. 3. Comparison of separate and integrated internal controls. HeLa cells (2.0×10^4/well in a 48-well plate) were treated with SARS#2 and pRL-TK (A), SARS#2, piGENE hU6, and pRL-TK (B), SARS#2, siRNA#2, and pRL-TK (C), SARS#2, siRNA#2 (100 ng/well), and pRL-TK (D), SARS#2-Rluc (E), SARS#2-Rluc and piGENE hU6 (F), SARS#2-Rluc and siRNA#2 (G), or SARS#2-Rluc and siRNA#2 (100 ng/well) (H). A concentration of 200 ng DNA/well was used for all vectors, unless otherwise indicated. As for vectors and target sequences, see Tables 1 and 2.

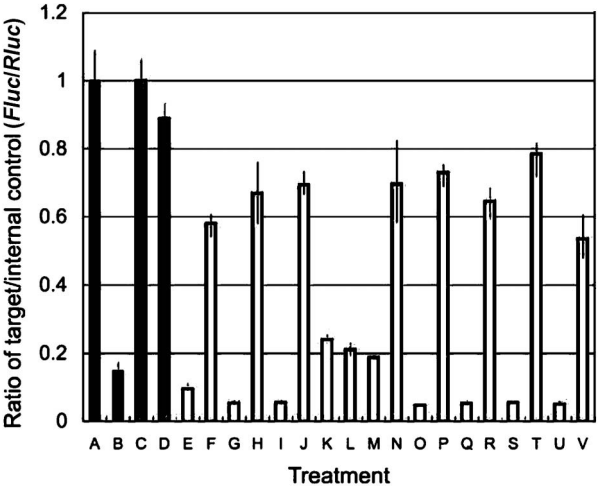

Fig. 4. Effects of dsRNA on normal SARS#1 and reverse R-SARS#1 targets. HeLa cells (2.0×10^4/well in a 48-well plate) were treated with SARS#1 and pRL-TK (A), SARS#1, siRNA#1, and pRL-TK (B), R-SARS#2 and pRL-TK (C), R-SARS#2, siRNA#2, and pRL-TK (D), SARS#1, ds-RNA [1]-[2], and pRL-TK (E), R-SARS#1, ds-RNA [1]-[2], and pRL-TK (F), SARS#1, ds-RNA [1]-[5], and pRL-TK (G), R-SARS#1, ds-RNA [1]-[5], and pRL-TK (H), SARS#1, ds-RNA [1]-[6], and pRL-TK (I), R-SARS#1, ds-RNA [1]-[6], and pRL-TK (J), SARS#1, ds-RNA [2]-[3], and pRL-TK (K), R-SARS#1, ds-RNA [2]-[3], and pRL-TK (L), SARS#1, ds-RNA [2]-[4], and pRL-TK (M), R-SARS#1, ds-RNA [2]-[4], and pRL-TK (N), SARS#1, ds-RNA [3]-[5], and pRL-TK (O), R-SARS#1, ds-RNA [3]-[5], and pRL-TK (P), SARS#1, ds-RNA [3]-[6], and pRL-TK (Q), R-SARS#1, ds-RNA [3]-[6], and pRL-TK (R), SARS#1, ds-RNA [4]-[5], and pRL-TK (S), R-SARS#1, ds-RNA [4]-[5], and pRL-TK (T), ds-RNA [4]-[6], and pRL-TK (U), or R-SARS#1, ds-RNA [4]-[6], and pRL-TK (V). A concentration of 100 ng DNA/well was used for SARS#1 and R-SARS#1, and that of 50 ng DNA/well, for pRL-TK. A concentration of 33 nM was used for dsRNA. The *Fluc/Rluc* ratios of treatments A (SARS#1 control) and C (R-SARS#1 control) are adjusted to be unity, and relative ratios of *Fluc/Rluc* are shown for other treatments. As for vectors and target sequences, see Tables 1 and 2. As for combinations of ds-RNA, see Table 3.

100 and 200 ng/well treatments, indicating that activities were saturated at 100 ng/well.

Effects of dsRNA on #1 normal and reverse targets: The siRNA activities of nine species of dsRNAs (Table 3) targeting their normal SARS#1 and reverse R-SARS#1 sequences are portrayed in Fig. 4. For comparison, siRNA expression vector DNA was also used. The siRNA#1 was effective for the SARS#1 target, but not effective for its opposite target, as expected. Most dsRNAs knocked down their normal targets (pale gray columns) more effectively than corresponding opposite targets (blank columns), except for the [2]-[3] combination, the sense strand of which has a 5′-blunt end and a 2-nt 3′-match overhang, suggesting preferential loading of the sense strand into RISC. From a quantitative viewpoint, however, overall knockdown activities of the [2]-[3] combination against the normal and opposite targets were lower than the other combinations. The most effective knockdown of the normal SARS#1 sequences was achieved by combinations including [5] or [6] (Table 3), which respectively have a 2-nt 3′-match and unmatch overhang in the antisense strand, suggesting the importance of the 2-nt overhang to be loaded into RISC.

Effects of dsRNA on #3 normal and reverse targets: The same experiment as portrayed in Fig. 4 was conducted using nine dsRNAs targeting the SARS#3 sequence, which starts from No. 17899 (Fig. 5). For comparison, siRNA expression vector DNA was used here again. As expected, the siRNA#3 was effective for the normal SARS#3 target, but not for its opposite target R-SARS#3. The siRNA#3 was generally more effective than SARS#1 (Figs. 1, 4 and 5), as predicted (Table 1). Some dsRNAs knocked down the normal and opposite targets almost equally; others did so more effectively for the normal target than the opposite one. Combinations containing [6], which has a 2-nt 3′-unmatch overhang in the antisense strand, were not effective in this case.

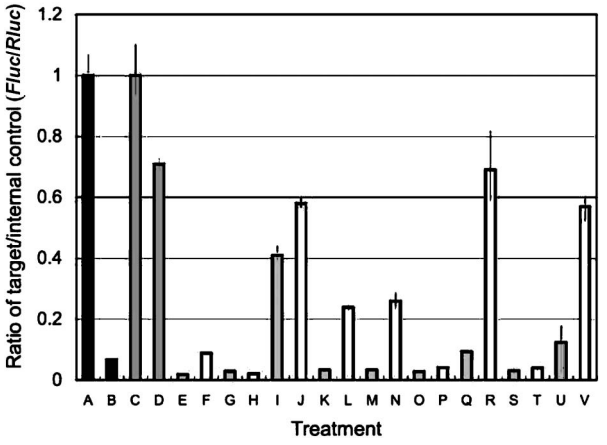

Fig. 5. Effects of dsRNA on normal SARS#3 and reverse R-SARS#3 targets. HeLa cells (2.0×10^4/well in a 48-well plate) were treated with SARS#3 and pRL-TK (A), SARS#3, siRNA#3, and pRL-TK (B), R-SARS#3 and pRL-TK (C), R-SARS#3, siRNA#3, and pRL-TK (D), SARS#3, ds-RNA [1]-[2], and pRL-TK (E), R-SARS#3, ds-RNA [1]-[2], and pRL-TK (F), SARS#3, ds-RNA [1]-[5], and pRL-TK (G), R-SARS#3, ds-RNA [1]-[5], and pRL-TK (H), SARS#3, ds-RNA [1]-[6], and pRL-TK (I), R-SARS#3, ds-RNA [1]-[6], and pRL-TK (J), SARS#3, ds-RNA [2]-[3], and pRL-TK (K), R-SARS#3, ds-RNA [2]-[3], and pRL-TK (L), SARS#3, ds-RNA [2]-[4], and pRL-TK (M), R-SARS#3, ds-RNA [2]-[4], and pRL-TK (N), SARS#3, ds-RNA [3]-[5], and pRL-TK (O), R-SARS#3, ds-RNA [3]-[5], and pRL-TK (P), SARS#3, ds-RNA [3]-[6], and pRL-TK (Q), R-SARS#3, ds-RNA [3]-[6], and pRL-TK (R), SARS#3, ds-RNA [4]-[5], and pRL-TK (S), R-SARS#3, ds-RNA [4]-[5], and pRL-TK (T), ds-RNA [4]-[6], and pRL-TK (U), or R-SARS#3, ds-RNA [4]-[6], and pRL-TK (V). A concentration of 100 ng DNA/well was used for SARS#3 and R-SARS#3, and that of 50 ng DNA/well, for pRL-TK. A concentration of 33 nM was used for dsRNA. The *Fluc/Rluc* ratios of treatments A (SARS#3 control) and C (R-SARS#3 control) are adjusted to be unity, and relative ratios of *Fluc/Rluc* are shown for other treatments. As for vectors and target sequences, see Tables 1 and 2. As for combinations of ds-RNA, see Table 3.

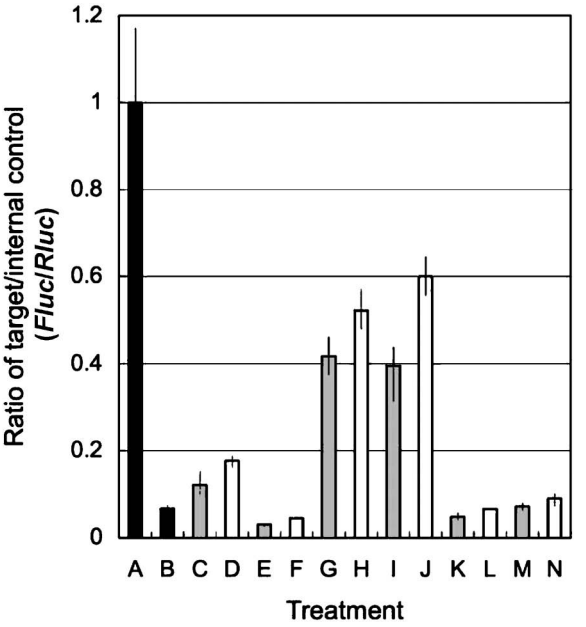

Fig. 6. Effects of dsRNAs on SARS#3 at lower dose levels. HeLa cells (2.0×10^4/well in a 48-well plate) were treated with SARS#3 and pRL-TK (A), SARS#3, siRNA#3, and pRL-TK (B), SARS#3, ds-RNA [1]-[2] (10 nM), and pRL-TK (C), SARS#3, ds-RNA [1]-[2] (3 nM), and pRL-TK (D), SARS#3, ds-RNA [1]-[5] (10 nM), and pRL-TK (E), SARS#3, ds-RNA [1]-[5] (3 nM), and pRL-TK (F), SARS#3, ds-RNA [2]-[3] (10 nM), and pRL-TK (G), SARS#3, ds-RNA [2]-[3] (3 nM), and pRL-TK (H), SARS#3, ds-RNA [2]-[4] (10 nM), and pRL-TK (I), SARS#3, ds-RNA [2]-[4] (3 nM), and pRL-TK (J), SARS#3, ds-RNA [3]-[5] (10 nM), and pRL-TK (K), SARS#3, ds-RNA [3]-[5] (3 nM), and pRL-TK (L), SARS#3, ds-RNA [4]-[5] (10 nM), and pRL-TK (M), or SARS#3, ds-RNA [4]-[5] (3 nM), and pRL-TK (N). A concentration of 100 ng DNA/well was used for SARS#3 and siRNA#3, and that of 50 ng DNA/well, for pRL-TK. The *Fluc/Rluc* ratio of treatment A (SARS#3 control) is adjusted to be unity, and relative ratios of *Fluc/Rluc* are shown for other treatments. As for vectors and target sequences, see Tables 1 and 2. As for combinations of ds-RNA, see Table 3.

Table 4. Thermodynamic stability (ΔG) at 4-bp terminal end of dsRNAs

Target site	Sequence	ΔG at the left end*	ΔG at the right end*	Matching steps/8 steps**
#1	5′-GCAUCGAUCUAAAGUCUUA-3′ 3′-CGUAGCUAGAUUUCAGAAU-5′	−2.7	−0.3	7
#2	5′-GCGUCUAACUAAAUACACA-3′ 3′-CGCAGAUUGAUUUAUGUGU-5′	−4.1	−2.3	6
#3	5′-AUAGAGAUCUUUAUGACAA-3′ 3′-UAUCUCUAGAAAUACUGUU-5′	−0.3	−1.4	6

*ΔG was calculated according to the equation shown in Ref. 26. **see Ref. 29.

The most effective and almost equal knockdown of the normal target was shown by combinations of [1]-[2], [1]-[5], [2]-[3], [2]-[4], [3]-[5], and [4]-[5] at a dose of 30 nM. Comparison of activities was difficult (Fig. 5). The siRNA activities might be saturated at this dose level; experimental results were obtained at 10 and 3 nM (Fig. 6). The marked feature is the combinations including [5], which showed highest activities. The order of effectiveness was [1]-[5] (m-b), [3]-[5] (m-m), and [4]-[5] (m-u) (Fig. 6 and Table 3), suggesting that a 2-nt 3′-match overhang in the antisense strand is critically important for this guide strand to be loaded into RISC. If thermodynamic stability at terminal ends is the major determinant of the strand selection, the present results (Figs. 5 and 6) are not explicable: the right end is more stable than the left end (Table 4), and the undesirable sense strand is expected to be loaded mainly into RISC in this case.

Discussion

As an attempt to control SARS CoV using RNAi technology, effective target sequences of siRNAs and structures of dsRNA were scrutinized using an siRNA expression vector (27) and synthetic dsRNA. We chose three target sequences that were not mutated among 15 strains of SARS CoV, three vectors were constructed, and their activities were measured. The activities were in the effective order of SARS#2 > SARS#3 > SARS#1 (Fig. 1) as predicted (Table 1), indicating that the prediction algorithm (21) is useful. The higher activity of SARS#3 over SARS#1 (Fig. 1) was supported not only by the siRNA expression vector system (compare plasmid data in Figs. 4 and 5), but also by the dsRNA system (compare dsRNA data in Figs. 4 and 5).

Because many factors are involved in the siRNA expression vector pathway, however, the use of synthetic dsRNAs is more convenient for detailed functional analyses. Small molecules are easily incorporated into cells. Especially, smaller duplexes (21-nt siRNAs) do not appear to bind Dicer *in vitro* (28), and the Dicer's action might be neglected. An empirical guide recommends 5′-AA(N_{19})UU in mRNA as a preferred target sequences (19). Based on results of analyses of 180 siRNAs targeting 197-nt region of *Fluc* (20), eight steps to silence targets have been proposed: 1) low G/C content (30–52%); 2) three or more A/U at the 3′-terminal of the sense strand; 3) a lack of internal repeats that can form secondary structures; 4) an A at position 19; 5) an A at position 3; 6) a U at position 10; 7) an absence of G or C at position 19; and 8) an absence of G at position 13 (29). A typical possible effective siRNA is the following (30).

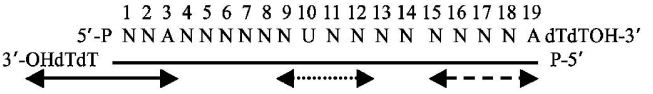

The solid-line arrow region shows that the 5′-sense strand terminus blocks must be thermodynamically stable. Furthermore, G/C is recommended at position 1 for the antisense strand to be loaded into RISC. The dotted-line arrow region promotes RISC-antisense strand mediated cleavage of mRNA and RISC-antisense strand complex release, and is preferably unstable. Low stability at the dashed-line arrow region is recommended for the antisense strand to be loaded into RISC. Matching step numbers among eight steps are presented in Table 4. Target site sequence #1 got a 7 score, but its siRNA activity was worst among the three, indicating that eight steps are insufficient to predict siRNA efficiency.

Among the eight steps, 2), 4), and 7) at least contribute to tightening the 5′-end and loosening the 3′-end of the sense strand. Indeed, the tight 5′-end and loose 3′-end of the sense strand was proposed as the deterministically important factor for the antisense strand to be loaded into RISC (22,23). The calculated thermodynamic stabilities of our strands (Table 4) showed that the left end of dsRNA#1 is more stable than the right end. The left stability seems to contribute to the preferential incorporation of the antisense strand (Fig. 4). However, the right end of dsRNA#3 is more stable than the left end (Table 4). Therefore, the thermodynamic stability cannot be the major determinant of the incorporation of the antisense strand. The higher activities were always shown by dsRNA including [5] (2-nt match 3′-overhang in the antisense strand) (Figs. 4–6). Therefore, this 2-nt overhang seems to be the

major determinant of guide strand selection to RISC. The order of siRNA efficiency among the three [5]-combinations was [1]-[5] > [3]-[5] > [4]-[5], although the differences were small (Fig. 6). The dsRNA [1]-[5] has a 2-nt 3′-overhang at the left end and is blunted at the right end. This structure of dsRNA is apparently the best, as we suggested in a previous report (24). The higher activity of dsRNA [1]-[5] over dsRNA [1]-[6] (Fig. 5) shows that the sequence of the overhang is expected to be complementary to the target mRNA.

The dsRNA of [1]-[5], [3]-[5], and [4]-[5] cleaved their targets, but these were also effective against the opposite target (Fig. 5). One possibility is that the sense strand derived from dsRNA of the #3 target site sequence is also effective against its target, in sharp contrast to the sequence #1, most sense strands derived from which were ineffective against their target (Fig. 4). The unstable left end of #3 (Table 4) might contribute to load the sense strand into RISC as a minor determinant. Since RNAi activities are sequence-dependent and sequence-specific, however, differences in the activities between synthetic dsRNAs derived from the sequences #1 and #3 (Table 1) must reside in their different sequences themselves, including relationship between overhang and stem sequences. Many factors are involved in the RNAi pathway to form functional RISC (31). Although we showed that a 2-nt match overhang at the 3′-end of the antisense strand is important to load this strand into RISC as a guide, evidence obtained by analyses of dsRNA sequences and their activities is quite limited. Different approaches, e.g., biochemical analyses of factors associated with the recognition of the 2-nt overhang at the 3′-end, are needed.

From practical viewpoints, we presented effective sequences such as #2 and #3 (Table 1) to knockdown SARS-Cov genes. Considering that SARS-Cov is a plus-strand RNA virus and produces minus-strand RNA during replication, dsRNAs [3]-[5] of the sequence #3 with 2-nt match overhangs at both ends are expected to be effective against plus-strand and minus-strand RNAs of SARS-Cov.

Acknowledgement: This study was supported in part by a grant to SS from Shujitsu University.

References

1 Drosten C, Günther S, Preiser W, van der Werf S, Brodt HR, Becker S, Rabenau H, Panning M, Kolesnikova L, Fouchier RA, Berger A, Burguière AM, Cinatl J, Eickmann M, Escriou N, Grywna K, Kramme S, Manuguerra JC, Müller S, Rickerts V, Stürmer M, Vieth S, Klenk HD, Osterhaus AD, Schmitz H, Doerr HW. Identification of a novel coronavirus in patients with severe acute respiratory syndrome. N Eng J Med. 2003; 348: 1967–76.

2 Ding Y, Wang H, Shen H, Li Z, Geng J, Han H, Cai J, Li X, Kang W, Weng D, Lu Y, Wu D, He L, Yao K. The clinical pathology of severe acute respiratory syndrome (SARS): a report from China. J Pathol. 2003; 200: 282–9.

3 SARS: What have we learned? Nature. 2003; 424: 121–6.

4 Fire A, Xu S, Montgomery MK, Kostas SA, Driver SE, Mello CC. Potent and specific genetic interference by double stranded RNA in *Caenorhabditis elegans*. Nature. 1998; 391: 806–11.

5 Elbashir SM, Harborth J, Lendeckel W, Yalcin A, Weber K, Tuschl T. Duplexes of 21-nucleotide RNAs mediate RNA interference in cultured mammalian cells. Nature. 2001; 411: 494–8.

6 Sasidharan R, Gerstein M. Protein fossils live on as RNA. Nature. 2008; 453: 729–31.

7 Bitko V, Barik S. Respiratory viral diseases: access to RNA interference therapy. Drug Discovery Today. 2007; 4: 273–6.

8 Elbashir SM, Martinez J, Patkaniowska A, Lendeckel W, Tuschl T. Functional anatomy of siRNAs for mediating efficient RNAi in *Drosophila melanogaster* embryo lysate. EMBO J. 2001; 20: 6877–88.

9 Sontheimer EJ. Assembly and function of RNA silencing complexes. Nat Rev Mol Cell Biol. 2005; 6: 127–38.

10 Tomari Y, Matranga C, Haley B, Martinez N, Zamore PD. A protein sensor for siRNA asymmetry. Science. 2004; 306: 1377–80.

11 Satija N, Lal SK. The molecular biology of SARS coronavirus. Ann N Y Acad Sci. 2007; 1102: 26–38.

12 Sutou S, Sato S, Okabe T, Nakai M, Sasaki N. Cloning and sequencing of genes encoding structural proteins of avian infectious bronchitis virus. Virology. 1988; 165: 589–95.

13 Zhang Y, Li T, Fu L, Yu C, Li Y, Xu X, Wang Y, Ning H, Zhang S, Chen W, Babiuk LA, Chang Z. Silencing SARS-CoV Spike protein expression in cultured cells by RNA interference. FEBS Lett. 2004; 560: 141–6.

14 Qin ZL, Zhao P, Zhang XL, Yu JG, Cao MM, Zhao LJ, Luan J, Qi ZT. Silencing of SARS-CoV spike gene by small interfering RNA in HEK293T cells. Biochem Biophys Res Commun. 2004; 324:1 186–93.

15 He ML, Zheng B, Peng Y, Peiris JSM, Poon LLM, Kwok YY, Lin MM, Kung HF, Guan Y. Inhibition of SARS-associated coronavirus infection and replication by RNA interference. JAMA. 2003; 290: 2665–6.

16 He ML, Zheng BJ, Chen Y, Wong KL, Huang JD, Lin MC, Peng Y, Yuen KY, Sung JJ, Kung HF. Kinetics and synergistic effects of siRNAs targeting structural and replicase genes of SARS-associated coronavirus. FEBS Lett. 2006; 580: 2414–20.

17 Meng B, Lui YW, Meng S, Cao C, Hu Y. Identification of effective siRNA blocking the expression of SARS viral envelope E and RDRP gene. Mol Biotechnol. 2006; 33: 141–8.

18 Li T, Zhang Y, Fu L, Yu C, Li X, Li Y, Zhang X, Rong Z, Wang Y, Ning H, Liang R, Chen W, Babiuk LA, Chang Z. siRNA targeting the leader sequence of SARS-CoV inhibits virus replication. Gene Ther. 2005; 12: 751–61.

19 Tuschl T. Targeting genes expressed in mammalian cells

using siRNAs. Nat Methods. 2004; June issue: 13–7.
20 Reynolds A, Leake D, Boese Q, Scaringe S, Marshall WS, Khvorova A. Rational siRNA design for RNA interference. Nat Biotechnol. 2004; 22: 326–30.
21 Taira K, Miyagishi M. Method and apparatus for predicting RNAi effect of siRNA. Japanese Patent No. 3642573. Feb. 4, 2005.
22 Khvorova A, Reynolds A, Jayasena SD. Functional siRNAs and miRNAs exhibit strand bias. Cell. 2003; 115: 209–16.
23 Schwarz DS, Hutvagner G, Du T, Xu Z, Aronin N, Zamore PD. Asymmetry in the assembly of the RNAi enzyme complex. Cell. 2003; 115: 199–208.
24 Sano M, Sierant M, Miyagishi M, Nakanishi M, Takagi Y, Sutou S. Effect of asymmetric terminal structures of short RNA duplexes on the RNA interference activity and strand selection. Nucleic Acid Res. 2008; doi:10.1093/nar/gkn584.
25 Sutou S, Kunishi M, Kudo T, Wongsrikeao P, Miyagishi M, Otoi T. Knockdown of the bovine prion gene PRNP by RNA interference (RNAi) technology. BMC Biotechnol. 2007; 7: 44 (http://www.biomedcentral.com/1472–6750/7/44).
26 Freier SM, Kierzek R, Jaeger JA, Sugimoto N, Caruthers MH, Neilson T, Turner DH. Improved free-energy parameters for predictions of RNA duplex stability. Proc Natl Acad Sci USA. 1986; 83: 9373–7.
27 Miyagishi M, Taira K. U6 promoter-driven siRNA with four uridine 3′- overhangs efficiently suppress targeted gene expression in mammalian cells. Nat Biotechnol. 2002; 20: 497–500.
28 Provost P, Dishart D, Doucet J, Frendewey D, Samuelsson B, Radmark O. Ribonuclease activity and RNA binding of recombinant human Dicer. EMBO J. 2002; 21: 5864–74.
29 Frantz S. Eight steps to scilence. Nat Rev. 2005; October: 4.
30 Mittal V. Improving the efficiency of RNA interference in mammals. Nat Rev. 2005; October: 29–39.
31 Sontheimer EJ. Assembly and function of RNA silencing complexes. Nat Rev Mol Cell Biol. 2005; 6: 127–38.